

# Genetic InfoMax: Exploring Mutual Information Maximization in High-Dimensional Imaging Genetics Studies

Anonymous authors

Paper under double-blind review

## Abstract

Genome-wide association studies (GWAS) are used to identify relationships between genetic variations and specific traits. When applied to high-dimensional medical imaging data, a key step is to extract lower-dimensional, yet informative representations of the data as traits. Representation learning for imaging genetics is largely under-explored due to the unique challenges posed by GWAS in comparison to typical visual representation learning. In this study, we tackle this problem from the mutual information (MI) perspective by identifying key limitations of existing methods. We introduce a trans-modal learning framework Genetic InfoMax (GIM), including a regularized MI estimator and a novel genetics-informed transformer to address the specific challenges of GWAS. We evaluate GIM on human brain 3D MRI data and establish standardized evaluation protocols to compare it to existing approaches. Our results demonstrate the effectiveness of GIM and a significantly improved performance on GWAS.

## 1 Introduction

Genome-wide association studies (GWAS) have been an effective approach driving genetic discovery in the past 15 years (Abdellaoui et al., 2023). Given a phenotype of interest and a cohort of individuals with both the measurements of the phenotype and the genotypes over markers across the genome, linear or linear mixed model are built to test for the association of each marker to the phenotype and thus pinpoint the relevant gene loci. However, the typical GWAS studies are focused on well-established phenotypes, typically the risks of diseases, or well-established macro-level measurements such as heights, BMI, or molecular-level measurements such as protein and metabolomic biomarkers. When the phenotype of interest is a high-dimensional complex data modality such as imaging data, there is a lack of sophisticated approaches for deriving phenotypes for GWAS. Taking brain imaging as an example, existing approaches mostly used traditional non-learning software to derive brain region-based volumetric or surface features. These approaches carry human preconceptions and biases, and thus limited the expressiveness of these phenotypes and the power of genetic discovery.

Recently deep learning approaches (Patel et al., 2022; Xie et al., 2022; Kirchler et al., 2022; Taleb et al., 2022) derive phenotypes from medical images by learning a latent representation that captures the inherent content of the input image. However, approaches learning from imaging data alone fail to utilize the accompanying genetic data. Those approaches tend to capture patterns that are not related to genes and common patterns shared by multiple individuals. For example, Patel et al. (2022) found that representations learned by an image autoencoder are unable to fully reconstruct fine details that are individually specific. To overcome these limitations, a solution is to incorporate trans-modal learning strategies that utilize the pairwise relationship between imaging and genetic data, such as trans-modal contrastive learning (Liang et al., 2022; Zolfaghari et al., 2021; Taleb et al., 2022). Unfortunately, the use of genetic data, including the encoding of data and capturing image-genetic relationships, still poses significant challenges. Results by Taleb et al. (2022) suggest that, despite the promising results for downstream classification of disease risk, multi-modal contrastive approaches still underperform compared to typical image-only approaches (Xie et al., 2022) on GWAS tasks. This underperformance becomes even more pronounced for higher-dimensional 3D data.

In this work, we formulate the problem as learning the representation of imaging data that shares the maximum mutual information with genetic data. By using mutual information as a perspective, we are able to examine the key reasons for the failure of typical trans-modal contrastive learning for GWAS on high-dimensional imaging data. To push the limits of existing learning approaches, we propose **Genetic InfoMax (GIM)**, a trans-modal learning framework that includes a regularized mutual information estimator and a novel transformer-based genetic encoder. The framework addresses the issues of dimensional collapse and non-generalizable associations in representation learning for GWAS, and fully utilizes the genetic data with physical and genetic position information. Our experiments demonstrate that GIM significantly improves performance on all four evaluation metrics.

## 2 Problem Formulation

We study the problem of genome-wide association studies (GWAS) on high-dimensional data. The GWAS aims to identify associations between specific genetic variants, known as single nucleotide polymorphisms (SNPs), in the genome and certain traits of interest such as the risk of disease and other biological characteristics of organisms. In particular, each individual genetic data is denoted by  $\mathbf{G} = \{\mathbf{g}_1, \dots, \mathbf{g}_L\}$ , and traits of interest denoted by  $\mathbf{y}$ , the GWAS process involves statistical tests on the sample pairs  $\{(\mathbf{G}_i, \mathbf{y}_i)\}_{i=1, \dots, M}$  from a large number of  $M$  individuals to identify the specific subset  $\mathbf{G}^{g \rightarrow y} \subset \mathbf{G}$  of SNPs that are associated with the target traits  $\mathbf{y}$ . Here  $L$  is the number of SNPs, each  $\mathbf{g}_i \in \{0, 1, 2\}$ , representing the number of carried variants for each individual. The values of nearby SNPs are often correlated due to their common inheritance from a shared ancestor. To account for this, it is necessary to select an independent subset of genetic information  $\mathbf{G}^{\text{ind}} \subset \mathbf{G}^{g \rightarrow y}$ , which can be achieved by clustering and selecting the SNPs with the lowest p-value from each cluster after the statistical test, which is important for accurate analysis and interpretation of the genetic data. Practically, when conducting GWAS on high-dimensional data  $\mathbf{Y}$  such as medical imaging, an additional step is required before performing statistical tests. This step involves reducing the number of traits from the high-dimensional data  $\mathbf{Y}$  to a smaller number  $\mathbf{y}$  through experts' diagnosis or computational approaches.

**Traits Computing as Representation Learning.** To enable GWAS on high-dimensional data, we are interested in computationally obtaining informative lower-dimensional traits, termed GWAS representation learning, from the high-dimensional data. Specifically, for any high-dimensional data  $\mathbf{Y}$  to be studied, the problem is formulated as to learn lower-dimensional representations of  $\mathbf{Y}$  with a corresponding encoder  $f_\theta$  in a self-supervised manner, such that a larger number of independent SNPs  $|\mathbf{G}^{\text{ind}}|$  can be identified from the pairs  $\{(\mathbf{G}_i, f_\theta(\mathbf{Y}_i))\}_{i=1, \dots, M}$ . The goal of identifying more independent SNPs requires that more information related to genetic variants is captured by the representation of  $\mathbf{Y}$ . We focus on learning  $d$ -dimensional representations  $\mathbf{y} = f_\theta(\mathbf{Y}) \in \mathbb{R}^q$  with the following optimization objective

$$\theta^* = \arg \max_{\theta} \mathcal{I}(f_\theta(\mathbf{Y}), \mathbf{G}), \quad (1)$$

where  $\mathcal{I}(\cdot, \cdot)$  denotes the mutual information (MI) between two random variables. As computing the true value of mutual information is intractable, it becomes critical to develop an appropriate mutual information estimation under the GWAS problem setting.

**Notations of Data.** We instantiate our problem specifically with the 3D human brain magnetic resonance imaging (MRI) data and SNPs from the human genome. We denote the 3D brain MRI by  $\mathbf{Y} \in \mathbb{R}^{H \times W \times D \times 1}$ , where  $H$ ,  $W$ ,  $D$  denote the three spatial dimensions, and 1 denotes the single channel of the MRI. The human genetic data  $\mathbf{G}$  consists of  $N$  positions on the human genome with frequent variants (SNPs). Each SNP  $\mathbf{g}_i$  is represented by a four-tuple  $(d_i, c_i, p_i^{\text{phy}}, p_i^{\text{gen}})$ . In the four-tuple,  $d_i \in \{0, 1, 2\}$  denotes the genotype of the SNP, the number of copies of the mutant allele,  $c_i \in \{1, \dots, 22\}$  denotes the index of chromosome the SNP belongs to,  $p_i^{\text{phy}} \in \mathbb{N}$  denotes the physical position in terms of base pair (bp) of the SNP in the chromosome, and  $p_i^{\text{gen}} \in \mathbb{R}^+$  denotes the genetic position of the SNP in terms of centimorgan (cM). Note that the genetic data is not a sequence but an array since two neighbor SNPs  $\mathbf{g}_i$  and  $\mathbf{g}_{i+1}$  are not necessarily to be consecutive on the original genome and the physical (and genetic) distance between them  $|p_i^{\text{phy}} - p_{i+1}^{\text{phy}}|$  is meaningful. We further denote arrays consisting of all genotypes, chromosomes, and positions sorted on chromosome id and physical position by  $\mathbf{d}$ ,  $\mathbf{c}$ ,  $\mathbf{p}^{\text{phy}}$ , and  $\mathbf{p}^{\text{gen}}$ , respectively.

### 3 What Makes Appropriate MI Estimators for GWAS?

With the goal of learning representations that capture as much information about the genetic variations as possible, our objective is to maximize the MI between the representation and genetic data with an appropriate MI estimator. One commonly used approach for estimating the mutual information between multi-dimensional variables is the Jensen-Shannon Estimator (JSE) (Nowozin et al., 2016). The JSE involves a discriminator to distinguish whether samples of the two variables belong to the same individual or are independently sampled. Specifically, under our problem setting, the JSE-based training loss is computed as

$$\begin{aligned} \mathcal{L}_{\text{JSE}}(\mathbf{B}; \theta, \phi) = & -\frac{1}{|\mathbf{B}|} \sum_{(\mathbf{Y}, \mathbf{G}) \in \mathbf{B}} \log \left( \mathcal{D}_{\phi}(f_{\theta}(\mathbf{Y}), \mathbf{G}) \right) \\ & - \frac{1}{|\mathbf{B}|(|\mathbf{B}| - 1)} \sum_{(\mathbf{Y}, \mathbf{G}) \in \mathbf{B}} \left[ \sum_{(\mathbf{Y}', \mathbf{G}') \in \mathbf{B} \setminus \{(\mathbf{Y}, \mathbf{G})\}} \log \left( 1 - \mathcal{D}_{\phi}(f_{\theta}(\mathbf{Y}), \mathbf{G}') \right) \right], \end{aligned} \quad (2)$$

where  $\mathbf{B}$  is a mini-batch of paired MRI and genetic data and  $\mathcal{D}_{\phi} : \mathbb{R}^q \times \mathcal{G} \rightarrow (0, 1)$  is a learnable discriminator to determine whether  $f_{\theta}(\mathbf{Y})$  and  $\mathbf{G}$  are from the same individual. Together with the Noise Contrastive Estimation (InfoNCE) (Bachman et al., 2019), these learning processes are also known to be in the contrastive manner across two modalities; namely, the MRI and genetic data.

To achieve desirable performance in maximizing MI and discovering genetic associations, the discriminator should meet certain requirements. First, the learnable discriminator  $\mathcal{D}_{\phi}$  should be able to take as inputs the genetic data  $\mathbf{G}$  and encode all the useful information from  $\mathbf{G}$ . A well-designed genetic encoder is thus a critical component of  $\mathcal{D}_{\phi}$ . It should be able to efficiently and effectively use not only the genotypes, but also their corresponding chromosome, physical position, and genetic position information. In Section 4, we propose a novel transformer-based genetic encoder, dubbed genetic transformer, that fully utilizes all this information based on genetic intuitions.

Second, the discriminator should make predictions based on all generalizably associated patterns, rather than memorizing noise or focusing on a small portion of associated patterns that can be easily learned. However, due to the nature of contrastive learning and several differences between typical visual representation learning and GWAS representation learning, we will argue below that it is challenging to meet this requirement. The typical contrastive loss can lead to degenerated results for GWAS as shown in Figure 1.

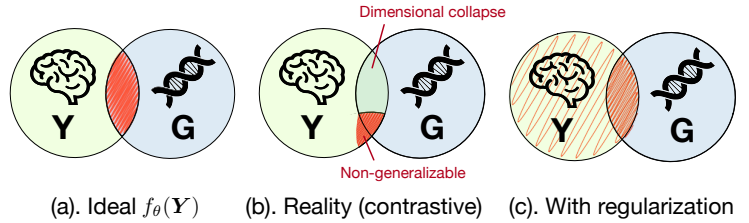


Figure 1: An illustration showing how the representation  $f_{\theta}(\mathbf{Y})$  captures the mutual information between  $\mathbf{Y}$  and  $\mathbf{G}$  in different cases. The circles are the entropy of  $\mathbf{G}$  and  $\mathbf{Y}$ , respectively, and their intersection is the mutual information  $\mathcal{I}(\mathbf{G}, \mathbf{Y})$ . Areas indicated by squiggles in red represent the information contained in  $f_{\theta}(\mathbf{Y})$ .

#### 3.1 Uniqueness of GWAS Representation Learning and Limitations of Contrastive Losses

To understand the limitations of typical contrastive losses in the GWAS setting, we first identify key differences between the visual representation learning problem for natural images and the GWAS representation learning on high-dimensional data. We explain how each difference can contribute to limitations or failures of typical contrastive losses in the GWAS setting, and provide empirical evidence to support our arguments.

**Difference 1: Goals of learning representations.** Typical visual representations of natural images aim to capture the key semantics or class information about major objects in images. With this goal, it is acceptable for the representation to capture only semantic or class-related information, or even required that representations are invariant to elements such as context (Zhang et al., 2021; Chang et al., 2021) and transformations (Xiao et al., 2020; Foster et al., 2020). In this case, a good representation for downstream tasks does not necessarily maximize the MI during contrastive learning. In contrast, a good representation for

the GWAS purpose should capture every detail or pattern in the high-dimensional MRI data that is associated with the genes, since there is no such key semantics or class information. In this case, the downstream GWAS performance is closely associated with  $\mathcal{I}(f_\theta(\mathbf{Y}), \mathbf{G})$ .

### Limitation 1: Dimensional collapse.

A recent study on visual representation learning (Jing et al., 2021) identifies and empirically shows that typical contrastive approaches suffer from the dimensional collapse issue, where the learned representations occupy a lower-dimensional subspace than their designated dimensions. The dimensional collapse results in high redundancy, limits the information captured by representations, and therefore leads to reduced performance in downstream tasks. Indeed, our analyses show that the dimensional collapse issue also presents in the cross-modal contrastive setting. We compare the singular values of representations learned by predictive methods and contrastive methods in Figure 2. Results indicate that the contrastive estimators NCE and JSE suffer from dimensional collapse with a dramatic drop in explained ratios and singular values. Even worse, the GWAS performance suffers more from the dimensional collapse issue due to its nature described in **Difference 1**, as both the information of  $f_\theta(\mathbf{Y})$  and the mutual information  $\mathcal{I}(f_\theta(\mathbf{Y}), \mathbf{G})$  is limited.

### Difference 2: Augmentation approaches and data dimensions.

Contrastive learning relies on a large number of samples to more accurately estimate and maximize the mutual information between different views or modalities. Previous studies (Chen et al., 2020; Tian et al., 2020) have shown that augmentations are crucial for contrastive learning, as they prevent representations from focusing on patterns that are irrelevant to downstream tasks and multiply the number of training samples. For higher-dimensional 3D MRI data, more samples and diverse augmentations are necessary (Vapnik, 1999). However, the availability of medical imaging data is limited, and most augmentations used for typical visual representation learning are not applicable to medical imaging. For example, since MRIs are single-channel, color space augmentations are not possible. Augmentations based on rotation and flipping are not suitable for brain MRI data due to their asymmetric nature. Random linear transform or non-linear morph may change the shape of the elements of the image and thus are discouraged. In the case of 3D MRI, the applicable augmentations are very limited.

**Limitation 2: Non-generalizable associations.** According to Huang et al. (2021), augmentations play a critical role in the generalization capability of contrastive learning approaches. However, due to the limited number of applicable augmentation techniques and the dimensionality of 3D data, the discriminator tends to

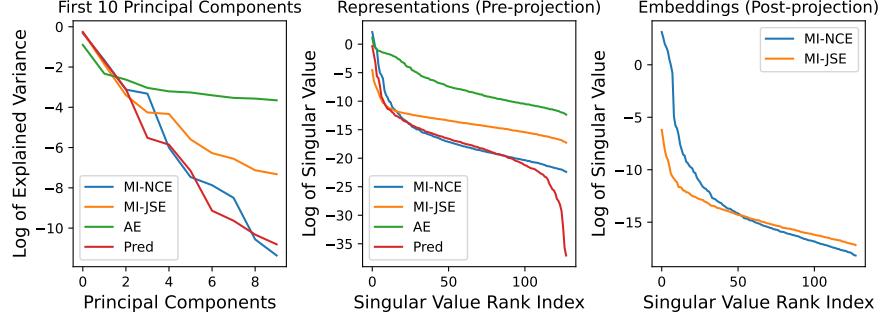


Figure 2: The logarithm of the explained variance for the first 10 principal components (**left**), the singular value spectrum of learned representations (**middle**) and embeddings after projection (**right**). Comparisons are among contrastive MI estimators with InfoNCE (MI-NCE), with JSE (MI-JSE), Autoencoder (AE), and genetic data prediction (Pred).

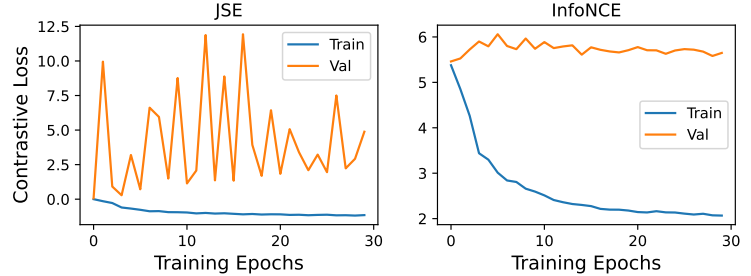


Figure 3: Generalization capability of contrastive MI estimators JSE (**left**) and InfoNCE (**right**). The learned discriminators fail to generalize to unseen pairs, leading to a large discrepancy between training and validation losses.

capture non-generalizable or false associations from the training samples such as memorizing the shape, the layout of the brain in the MRI, or specific noise in the data to identify individuals. In Figure 3, we evaluate the generalizability of models trained with contrastive loss by comparing the MI estimation on training and validation pairs. The remarkable discrepancy in losses between the training and validation sets suggests that the discriminator used by contrastive loss is unable to generalize to new samples, indicating that contrastive loss is a poor estimation of MI in our case.

From the perspective of mutual information, due to the dimensional collapse, a limited amount of training samples, sufficient means of augmentations, empirical results show that the JSE is not an optimal estimator of mutual information. The true mutual information is hence not maximized by the learned representations, leading to degraded performance in GWAS. Figure 1 (a–b) illustrates the relationship among the brain MRI, genetic data, and the learned representation. In the ideal case shown in (a), the representation should perfectly cover the mutual information between  $\mathbf{Y}$  and  $\mathbf{G}$ , so that the learning objective achieves its maximal with

$$\mathcal{I}(f_\theta(\mathbf{Y}), \mathbf{G}) = \mathcal{I}(\mathbf{Y}, \mathbf{G}) \geq \mathcal{I}(f_{\theta'}(\mathbf{Y}), \mathbf{G}), \forall f_{\theta'}. \quad (3)$$

In practice with brain MRI data, the contrastive loss results in representations that only capture a small portion of  $\mathcal{I}(\mathbf{Y}, \mathbf{G})$  due to the two limitations described above, as shown in (b).

### 3.2 MI Estimator with Regularizations

Given the issues and limitations outlined above, our goal is to improve the representation by incorporating more generalizably associated patterns in addition to those identified by the contrastive MI estimator. However, unlike in the case of natural images where many elements are known to be non-generalizable, our limited knowledge of undiscovered genetic associations makes it difficult to determine which patterns are generalizable and which are not. As a result, it is challenging to develop targeted augmentations that make the representation invariant to unwanted patterns.

To achieve our goal without requiring further knowledge, we propose to uniformly increase the total information contained in the representation by including an entropy term in the learning objective. The objective is formulated as

$$\max_{\theta} \left[ \hat{\mathcal{I}}(f_\theta(\mathbf{Y}), \mathbf{G}) + \lambda H(f_\theta(\mathbf{Y})) \right], \quad (4)$$

where  $\hat{\mathcal{I}}$  is the contrastive MI estimation JSE,  $H$  denotes the entropy of a random variable, and  $\lambda$  is a weight scalar. The entropy term encourages the representation to capture more information about  $\mathbf{Y}$  and reduces its redundancy. A certain portion of the information can contribute to the generalizable associations, as illustrated in Figure 1-(c). The entropy term serves as a regularization to the estimated MI to improve its generalizability. From the optimization aspect of view, the objective is considered as adding a Lagrange multiplier to maximize the entropy  $H(f_\theta(\mathbf{Y}))$ , subject to the constraint that the estimated mutual information  $\hat{\mathcal{I}}(f_\theta(\mathbf{Y}), \mathbf{G})$  achieves its maximum. When multiple patterns can be used to identify individuals, the entropy term encourages the model to capture as many of them as possible, instead of capturing the easiest ones.

There are various methods to estimate and optimize the entropy, such as minimizing the off-diagonal values in the covariance matrix of the representation (Zbontar et al., 2021). However, these estimations require a large mini-batch size, which is not suitable in our case due to memory constraints caused by the 3D data and MRI encoder. As an alternative, we use the reconstruction of MRI data as a proxy to maximize the entropy. The loss is then computed as

$$\mathcal{L}(\mathbf{B}; \theta, \phi, \psi) = \mathcal{L}_{\text{JSE}}(\mathbf{B}; \theta, \phi) + \frac{\lambda}{|\mathbf{B}|} \sum_{(\mathbf{Y}, \mathbf{G}) \in \mathbf{B}} \|\mathbf{Y} - h_\psi(f_\theta(\mathbf{Y}))\|^2, \quad (5)$$

where  $h_\psi$  is a deterministic decoding head used to reconstruct the MRI from the representation  $f_\theta(\mathbf{Y})$ . Compared to other proxies discussed by Zbontar et al. (2021), the reconstruction term is less sensitive to small mini-batch sizes. To justify the reconstruction term, we have

$$H(f_\theta(\mathbf{Y})) = \mathcal{I}(f_\theta(\mathbf{Y}), \mathbf{Y}) + \overbrace{H(f_\theta(\mathbf{Y})|\mathbf{Y})}^{\rightarrow 0}, \quad (6)$$

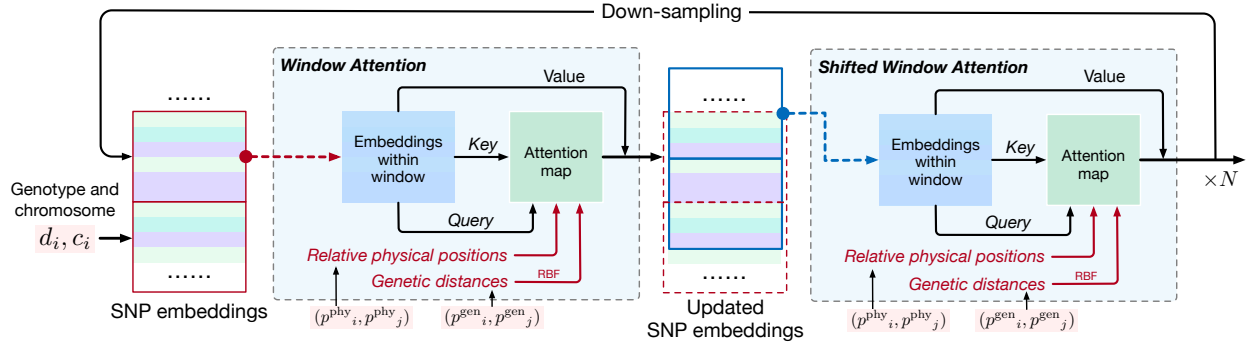


Figure 4: A swin-transformer block in the proposed genetic encoder. Red and blue boxes represent the windows and shifted windows.

and the reconstruction term is to maximize the log-likelihood that  $f_\theta(\mathbf{Y})$  and  $\mathbf{Y}$  in a positive pair belong to the same individual, similarly to the first term in the right-hand side (RHS) of Eq. (2). From the perspective of Wang and Isola (2020), the two terms in  $\mathcal{L}_{\text{JSE}}(\mathbf{B}; \theta, \phi)$  and the reconstruction term aim at three properties of  $f_\theta(\mathbf{Y})$ ; namely, the alignment to  $\mathbf{G}$ , the uniformity, and the alignment to  $\mathbf{Y}$ , respectively. As the uniformity of  $f_\theta(\mathbf{Y})$  is encouraged by the estimation of  $\mathcal{I}(f_\theta(\mathbf{Y}), \mathbf{G})$ , we omit the corresponding term in the estimation of  $\mathcal{I}(f_\theta(\mathbf{Y}), \mathbf{Y})$  for memory efficiency.

## 4 Genetics-Informed Transformer

A typical current genotyping microarray of the human genome includes more than 650k SNPs, with the physical spacing between any two consecutive SNPs being inconsistent. Genetic encoders developed in existing studies (van Hilten et al., 2021; Taleb et al., 2022) based on convolutional neural networks (CNNs) and multi-layer perceptrons (MLPs) are incapable of handling the unstructured genetic data with extremely large sizes. To address this, we develop an effective genetics-informed transformer to encode genetic data in accordance with the following objectives:

1. Significant optimized computational cost, in recognition of certain biological assumptions.
2. Information aggregation among SNPs from arbitrary positions in the genome, considering multiple genetics dependency measurements.
3. Flexibility to accept any segments or subsets of the genetic data as input, thereby facilitating cropping or downsampling-based augmentations on the genetic data.

An overview of the proposed transformer block is shown in Fig. 4, where attention operators with shifting windows (Liu et al., 2021) are used to enable efficient computation, and the aggregation is specialized with both physical and genetic distances of SNPs. In the transformer, two blocks are connected by down-sampling with attention-based pooling operators, and the initial SNP embeddings are computed based on both the genotypes and the chromosome each SNP belongs to. Finally, an attention-based readout is used to compute the global representation.

**Window attention in swin-transformer.** The 1D swin-transformer performs self-attention operations within each window split from the entire genetic array to enable efficient computing. It contains two components; those are, window attention and shifted window attention, as shown in Fig. 4. Given input SNP embeddings  $\mathbf{H} \in \mathbb{R}^{L \times q}$  where  $L$  denotes the number of SNPs and  $q$  denotes the embedding dimension, window attention first splits  $\mathbf{H}$  into a set of windows  $\{\mathbf{H}_i \in \mathbb{R}^{w \times q}\}_{i=1, \dots, \lfloor L/w \rfloor}$  where each window has a size  $w$ . A self-attention block is then applied to each  $\mathbf{H}_i$  to update the SNP embeddings by aggregating information within that window. The updated windows are then merged back following the order when splitting  $\mathbf{H}$ , forming  $\mathbf{H}'$  as the final output of the window attention component. In the following shifted window attention component,  $\mathbf{H}'$  is first shifted by a length of  $\lfloor w/2 \rfloor$ . Then similar splitting and self-attention are performed as in window attention to update SNP embeddings from each individual window. Finally, the updated windows are merged back, and the merged sequence is also shifted back by a length of  $\lfloor w/2 \rfloor$ . There exists a biological assumption that strong and informative dependencies between SNPs exist only when they

are within a certain distance. Hence, compared with performing global attention on all 650k marker positions, performing attention within windows in our proposed methods aggregates similar information, but largely reduces the computing cost.

**Aggregation based on multiple dependencies.** Multiple attention heads are computed to capture various types of dependencies among markers. Specifically, the computing of attention scores captures dependencies from three perspectives; those are, the SNP embeddings reflecting potential co-mutation, the encodings of the physical positions of SNPs on a chromosome indicating local dependencies among SNPs, and the encodings of genetic positions of SNPs measuring genetic linkages. Formally, the attention score  $\alpha_{i,j}^k$  between the  $i$ -th and  $j$ -th SNPs for the  $k$ -th attention head is computed as

$$\alpha_{i,j}^k = f_{\alpha}^k(\mathbf{g}_i, \mathbf{g}_j) = f_{\alpha_g}^k(\mathbf{h}_i, \mathbf{h}_j) + f_{\alpha_p}^k(p_i^{\text{phy}}, p_j^{\text{phy}}) + f_{\text{RBF}}^k(p_i^{\text{gen}} - p_j^{\text{gen}}), \quad (7)$$

where  $\mathbf{h}_i = \mathbf{H}[i] \in \mathbb{R}^q$  denote the SNP embedding. We compute the three individual components of attention scores that can capture different genetic dependencies as

$$\begin{aligned} f_h^k(\mathbf{h}_i, \mathbf{h}_j) &= \left( \mathbf{h}_i^T \mathbf{W}_h^{k,l} \right) \left( \mathbf{h}_j^T \mathbf{W}_h^{k,r} \right)^T, f_{\text{pe}}^k(p_i^{\text{phy}}, p_j^{\text{phy}}) = \left[ \mathbf{e}_p(p_i^{\text{phy}})^T \mathbf{W}_{\text{pe}}^{k,l} \right] \left[ \mathbf{e}_p(p_j^{\text{phy}})^T \mathbf{W}_{\text{pe}}^{k,r} \right]^T, \\ f_{\text{RBF}}^k(p_i^{\text{gen}} - p_j^{\text{gen}}) &= \left[ \mathbf{r}(|p_i^{\text{gen}} - p_j^{\text{gen}}|) \right]^T \left[ \mathbf{1}_{(p_i^{\text{gen}} - p_j^{\text{gen}}) \geq 0}^T \mathbf{W}_{\text{rbf}}^{k,+} + \mathbf{1}_{(p_i^{\text{gen}} - p_j^{\text{gen}}) < 0}^T \mathbf{W}_{\text{rbf}}^{k,-} \right], \end{aligned} \quad (8)$$

where  $\mathbf{e}_p(\cdot)$  denotes the position encoding (Devlin et al., 2019),  $\mathbf{W}_g^{k,l}$ ,  $\mathbf{W}_g^{k,r}$ ,  $\mathbf{W}_{\text{pe}}^{k,l}$ ,  $\mathbf{W}_{\text{pe}}^{k,r}$ , and  $\mathbf{W}_{\text{rbf}}^{k,+}$ ,  $\mathbf{W}_{\text{rbf}}^{k,-}$  are trainable projections.  $\mathbf{1}_{\text{condition}}^T$  is an indicator vector where all elements are 1s if the condition holds, and are 0s otherwise. The function  $\mathbf{r}$  denotes a distance expansion with radial basis functions (RBF) (Schütt et al., 2017). Denoting  $s := |p_i^{\text{gen}} - p_j^{\text{gen}}|$ , the term  $\mathbf{r}(|p_i^{\text{gen}} - p_j^{\text{gen}}|)$  in the above equation is computed as

$$\mathbf{r}(s) = \left[ \exp \left\{ (s - t)^2 / \sigma^2 \right\} \right]_{t \in \{t_0, \dots, t_c\}} \in \mathbb{R}^c, \quad (9)$$

where  $\{t_0, \dots, t_c\}$  is a set of non-negative real numbers ranging from 0 and a preset threshold. The asymmetric projections in all  $f_h, f_{\text{pe}}$  and  $f_{\text{RBF}}$  functions indicate that  $\alpha_{i,j}$  does not necessarily equal to  $\alpha_{j,i}$ , leading to more expressive models to capture dependencies. In addition, the computing of each attention head is based on a combination of three types of dependencies, which enables information aggregation among different SNPs based on genetic dependencies. By doing this, the complicated genetic dependencies of the input genome data can be captured. Additional details about the transformer are provided in Appendix B.

## 5 Related Work

**Dimension reduction for GWAS.** When doing genome-wide association studies, people oftentimes find themselves dealing with high-dimensional quantitative traits. In order to reduce computational cost and redundancy, and in the hope of finding meaningful underlying patterns, many works perform dimension reduction of the high dimensional traits before doing GWAS, including principal component analysis (Zhao et al., 2021; Yano et al., 2019; Ma et al., 2021), independent component analysis (Elliott et al., 2018; Pearlson et al., 2015) and non-negative matrix factorization (Wen et al., 2022). These approaches are effective in capturing linear dependencies but are less capable of identifying complicated traits from imaging data.

**Deep learning-based approaches.** Recently, several works used unsupervised learning to characterize high-dimensional medical data. iGWAS (Xie et al., 2022) applied contrastive learning between multiple images of the same person to reveal potential genetic signals, ContIG (Taleb et al., 2022) applied contrastive learning between medical imaging data and genetic data to learn the feature representation. DeepEndo autoencoder (Patel et al., 2022) used a convolutional autoencoder to reduce the dimensionality of the imaging data and found genetic associations of these extracted phenotypes. TransferGWAS (Kirchler et al., 2022) used both supervised task and reconstruction task to learn the feature representation. Specifically, ContIG (Taleb et al., 2022) is the first to use contrastive learning between images and genetics on the GWAS problem. However, there are distinguishable differences between the work and ours. First, ContIG aims to learn general representation for multiple downstream tasks, such as classifications of the risk of several diseases. With

Table 1: Comparisons of quantitative evaluation results on the test set. # Loci are counted under Bonferroni corrected p-value threshold (cutoff) of  $5e-9$ . “Unique” refers to the number of loci discovered by a method that is NOT discovered by any methods in other groups.

	Methods	# <i>Independent Loci</i>		Estimated MI $\uparrow$	Heritability $h^2 \uparrow$
		All $\uparrow$	Unique $\uparrow$		
<i>Predictive</i>	Random Init	14	1	1.2165	$0.0756 \pm 0.0656$
	Autoencoder (Patel et al., 2022)	26	1	1.3120	$0.3121 \pm 0.0769$
	Autoencoder-attention	23	4	1.3124	$0.2984 \pm 0.0773$
	Gen Prediction	10	0	1.2412	$0.0918 \pm 0.1110$
<i>Contrastive</i>	Barlow Twins (Zbontar et al., 2021)	11	1	1.2996	$0.0814 \pm 0.0636$
	SimCLR (Chen et al., 2020)	15	1	1.2397	$0.1448 \pm 0.1128$
	SimCLR-JSE	17	7	1.3044	$0.1604 \pm 0.1151$
<i>Trans-Modal Contrastive</i>	InfoNCE (ContIG, Taleb et al. (2022))	11	0	1.2299	$0.1334 \pm 0.0588$
	Decorrelated InfoNCE	13	3	1.2382	$0.0527 \pm 0.0349$
	GIM (Ours)	<b>40</b>	<b>15</b>	<b>1.3681</b>	<b><math>0.3723 \pm 0.0305</math></b>

this goal, ContIG treats the problem as a typical visual representation learning task. On the contrary, our study focuses on the representation learning specifically for GWAS. Second, our approaches are built upon the grounding of mutual information maximization, whereas ContIG is grounded by contrastive learning for unlabelled data. Third, our work focuses on a more challenging setting with 3D MRI data, where typical contrastive approaches may fail.

**Mutual Information Maximization.** Previous research has employed mutual information maximization as a pretext task for representation learning on various data types, including images (Hjelm et al., 2019), videos (Hjelm and Bachman, 2020), and graphs (Velićković et al., 2019; Stärk et al., 2022). However, these studies primarily focus on classification or regression as downstream tasks. Our work presents unique challenges and goals of mutual information maximization under the GWAS setting and we are the first to examine GWAS from a mutual information perspective.

## 6 Experiments

We use the brain imaging dataset from UK Biobank (Sudlow et al., 2015) in this study, it is currently the largest public brain imaging dataset. Specifically, we use T1-weighted MRI imaging data accessed on October 15, 2021. We register and pre-process the MRI data into the shape of  $182 \times 218 \times 182$ . For representation learning, we split the MRI-genetic data pairs into 4,597 training and 1,533 validation pairs based on ethnicity. A detailed description of the processing and split is provided in Appendix A.

**GWAS Evaluation Metrics** We involve three metrics to evaluate the representations learned by different models; namely, the **number of loci** discovered by GWAS, the **estimated mutual information**, and the **heritability** of the representations. All three metrics are computed on a testing dataset that is unseen during the representation learning process and measures the quality of representation for GWAS purposes. To enable efficient evaluation, we obtain the first 10 principal components of representations and compute all metrics on the 10-dimensional vectors. We provide detailed descriptions of each evaluation metric in Appendix A.

### 6.1 Quantitative Results and Analysis

We compare our approach with multiple baseline approaches in four groups; namely, MRI encoders that are randomly initialized, trained by predictive approaches, contrastive approaches with MRI data only, and trans-modal contrastive approaches that involves genetic data. The baselines include existing or straightforward training schemes Autoencoder (Kirchler et al., 2022; Patel et al., 2022), **Gen Prediction** that uses genetic data prediction as a pretext task, Barlow-Twins (Zbontar et al., 2021), SimCLR (Chen et al., 2020), and ContIG (Taleb et al., 2022). We additionally include their variants **Autoencoder-attention** that uses the same MRI encoder as ours, **SimCLR-JSE**, where the contrastive objective in SimCLR is replaced by JSE, and **Decorrelated InfoNCE**, where a decorrelation term is added to the contrastive loss. We describe the implementation details of GIM and baselines in Appendix B.



Table 2: Change in the number of loci and heritability when incrementally adding components to the models.

Methods	# Loci	Change	# Unique Loci	Change	$h^2$	Significant Gene
Base-Contrastive	11	-	0	-	0.1334	-
+ Regularization	29	+18	6	+6	0.3390	<i>CENPW</i>
+ Genetic Transformer	32	+5	10	+4	0.3773	<i>WNT16</i>
+ Random Cropping	36	+4	13	+3	0.3807	<i>ITPR3</i>
+ Co-training	40	+4	15	+2	0.3723	<i>MSRB3</i>

Comparisons among representations learned by different methods in terms of the three metrics are shown in Table 1. The results indicate that the proposed learning framework with regularized MI estimator and genetic transformer significantly improves the quality of learned representation in terms of the number of discovered loci and the heritability. The improved MI of our methods on test pairs also suggests a stronger generalization capability. Additionally, we have the following observations.

**The level of mutual information on test pairs agrees with # loci and heritability.** The results suggest that higher mutual information on the test set implies a higher heritability and more loci discovered. It justifies our formulation of learning representation for GWAS as the problem of maximizing mutual information.

**Typical trans-modal contrastive approaches fail for MRI data.** Trans-modal contrastive learning with typical contrastive loss performs fairly well on 2D retina imaging (Taleb et al., 2022) but suffers more from the performance reduction on the higher-dimensional 3D data. In the 3D MRI case, we found that the simplest Autoencoder approach performs even better than contrastive and typical trans-modal contrastive approaches.

## 6.2 Ablations and Additional Results

We perform additional quantitative studies to demonstrate the effectiveness of GIM. Visualizations for representation uniformity and Manhattan plot for GWAS are provided in Appendices C, D, and E.

**Effectiveness of individual proposed components.** To show the effectiveness and necessity of both the proposed learning objective and the genetic transformer, we track the change in the number of all loci, unique loci, the heritability score, and newly discovered genes with the highest significance when incrementally adding each component. Table 2 shows the results of adding the regularization to the objective, replacing the MLP encoder with the genetics-informed transformer, and performing random cropping on the genetic data. The results suggest that adding each component generally increase the useful information carried by the representations, leading to more loci discovered. We discuss the new gene discovered by each component and the change of  $h^2$  in Appendix D.

**GWAS representation for T2-weighted MRI.** We additionally apply GIM to a second modality, namely the T2-weighted MRI. Similarly, we compute GWAS on the first 10 principle components of the learned representation on the test set. In contrast to the results for T1, we observe that learning informative representations is less challenging for contrastive methods in the T2 case. In addition, contrastive methods equipped with NCE generally perform better than their JSE counterparts. This result is consistent with those presented in (Taleb et al., 2022). Nevertheless, results in Table 3 show a consistent out-performance of GIM over baselines, indicating generalizable effectiveness.

Table 3: # Loci for T2-weighted MRI at cutoffs 5e-9 and 1e-8.

Methods	5e-9	1e-8
Autoencoder	29	48
Barlow-Twin	7	14
SimCLR	21	28
SimCLR-JSE	15	20
ContIG	22	29
GIM (Ours)	<b>38</b>	<b>62</b>

Table 4: ROC-AUC of downstream classification.

Methods	Stroke	Cancer	Sex
Autoencoder	0.5353	<b>0.5971</b>	0.7357
SimCLR	0.5216	0.5216	0.5944
ContIG	0.6172	0.5689	0.7383
GIM (Ours)	<b>0.6381</b>	0.5750	<b>0.8641</b>

**Downstream classification performance.** Although being not our primary goal, we perform additional evaluation with three downstream classification tasks, namely stroke, cancer, and sex, from UK Biobank. We follow ContIG to perform linear evaluation protocol and compute their ROC-AUC, shown in Table 4. GIM achieves on par or better performance compared to its contrastive counterparts.

## 7 Conclusions

We have investigated the differences and limitations of GWAS representation learning compare to typical visual representation learning and have presented Genetic InfoMax, a GWAS representation learning framework. We have established standardized evaluation protocols to benchmark existing and our approaches. Our experiments demonstrate a significant boost in GWAS performance by GIM. We discuss the limitations of our work and future directions in Appendix F.

## References

- Abdel Abdellaoui, Loic Yengo, Karin JH Verweij, and Peter M Visscher. 15 years of gwas discovery: Realizing the promise. *The American Journal of Human Genetics*, 2023.
- Stephanie L Adams, Laurent Benayoun, Kathy Tilton, Olivia R Chavez, Jayandra J Himali, Jan Krzysztof Blusztajn, Sudha Seshadri, and Ivana Delalle. Methionine sulfoxide reductase-b3 (msrb3) protein associates with synaptic vesicles and its expression changes in the hippocampi of alzheimer’s disease patients. *Journal of Alzheimer’s Disease*, 60(1):43–56, 2017.
- Nil Aygün, Angela L Elwell, Dan Liang, Michael J Lafferty, Kerry E Cheek, Kenan P Courtney, Jessica Mory, Ellie Hadden-Ford, Oleh Krupa, Luis de la Torre-Ubieta, et al. Brain-trait-associated variants impact cell-type-specific gene regulation during neurogenesis. *The American Journal of Human Genetics*, 108(9):1647–1668, 2021.
- Philip Bachman, R Devon Hjelm, and William Buchwalter. Learning representations by maximizing mutual information across views. *Advances in neural information processing systems*, 32, 2019.
- Brendan Bulik-Sullivan, Hilary K Finucane, Verner Anttila, Alexander Gusev, Felix R Day, Po-Ru Loh, Laramie Duncan, John RB Perry, Nick Patterson, Elise B Robinson, et al. An atlas of genetic correlations across human diseases and traits. *Nature genetics*, 47(11):1236–1241, 2015.
- Judit Cabana-Domínguez, Bàrbara Torrico, Andreas Reif, Noèlia Fernández-Castillo, and Bru Cormand. Comprehensive exploration of the genetic contribution of the dopaminergic and serotonergic pathways to psychiatric disorders. *Translational Psychiatry*, 12(1):11, 2022.
- Chun-Hao Chang, George Alexandru Adam, and Anna Goldenberg. Towards robust classification model by counterfactual and invariant data generation. In *Proceedings of the IEEE/CVF Conference on Computer Vision and Pattern Recognition*, pages 15212–15221, 2021.
- Ting Chen, Simon Kornblith, Mohammad Norouzi, and Geoffrey Hinton. A simple framework for contrastive learning of visual representations. In *Proceedings of the International Conference on Machine Learning*, 2020.
- Jacob Devlin, Ming-Wei Chang, Kenton Lee, and Kristina Toutanova. BERT: pre-training of deep bidirectional transformers for language understanding. In *Proceedings of the 2019 Conference of the North American Chapter of the Association for Computational Linguistics: Human Language Technologies*, pages 4171–4186, 2019.
- Lloyd T Elliott, Kevin Sharp, Fidel Alfaro-Almagro, Sinan Shi, Karla L Miller, Gwenaëlle Douaud, Jonathan Marchini, and Stephen M Smith. Genome-wide association studies of brain imaging phenotypes in uk biobank. *Nature*, 562(7726):210–216, 2018.
- Adam Foster, Rattana Pukdee, and Tom Rainforth. Improving transformation invariance in contrastive representation learning. In *International Conference on Learning Representations*, 2020.
- Francesca Gori, Ulf Lerner, Claes Ohlsson, and Roland Baron. A new wnt on the bone: Wnt16, cortical bone thickness, porosity and fractures. *BoneKEy reports*, 4:669, 2015.
- R Devon Hjelm and Philip Bachman. Representation learning with video deep infomax. *arXiv preprint arXiv:2007.13278*, 2020.

- R Devon Hjelm, Alex Fedorov, Samuel Lavoie-Marchildon, Karan Grewal, Phil Bachman, Adam Trischler, and Yoshua Bengio. Learning deep representations by mutual information estimation and maximization. In *International Conference on Learning Representations*, 2019.
- Weiran Huang, Mingyang Yi, and Xuyang Zhao. Towards the generalization of contrastive self-supervised learning. *arXiv preprint arXiv:2111.00743*, 2021.
- Mark Jenkinson, Peter Bannister, Michael Brady, and Stephen Smith. Improved optimization for the robust and accurate linear registration and motion correction of brain images. *Neuroimage*, 17(2):825–841, 2002.
- Li Jing, Pascal Vincent, Yann LeCun, and Yuandong Tian. Understanding dimensional collapse in contrastive self-supervised learning. In *International Conference on Learning Representations*, 2021.
- Diederik P Kingma and Jimmy Ba. Adam: A method for stochastic optimization. *arXiv preprint arXiv:1412.6980*, 2014.
- Matthias Kirchlner, Stefan Konigorski, Matthias Norden, Christian Meltendorf, Marius Kloft, Claudia Schurmann, and Christoph Lippert. transferGwas: Gwas of images using deep transfer learning. *Bioinformatics*, 38(14):3621–3628, 2022.
- Weixin Liang, Yuhui Zhang, Yongchan Kwon, Serena Yeung, and James Zou. Mind the gap: Understanding the modality gap in multi-modal contrastive representation learning. In *Advances in Neural Information Processing Systems*, 2022.
- Ze Liu, Yutong Lin, Yue Cao, Han Hu, Yixuan Wei, Zheng Zhang, Stephen Lin, and Baining Guo. Swin transformer: Hierarchical vision transformer using shifted windows. In *Proceedings of the IEEE/CVF International Conference on Computer Vision (ICCV)*, 2021.
- Po-Ru Loh, George Tucker, Brendan K Bulik-Sullivan, Bjarni J Vilhjalmsdsson, Hilary K Finucane, Rany M Salem, Daniel I Chasman, Paul M Ridker, Benjamin M Neale, Bonnie Berger, et al. Efficient bayesian mixed-model analysis increases association power in large cohorts. *Nature genetics*, 47(3):284–290, 2015.
- Ilya Loshchilov and Frank Hutter. Sgdr: Stochastic gradient descent with warm restarts. *arXiv preprint arXiv:1608.03983*, 2016.
- Langlang Ma, Chunyan Qing, Minyan Zhang, Chaoying Zou, Guangtang Pan, and Yaou Shen. Gwas with a pca uncovers candidate genes for accumulations of microelements in maize seedlings. *Physiologia Plantarum*, 172(4):2170–2180, 2021.
- Jacqueline MacArthur, Emily Bowler, Maria Cerezo, Laurent Gil, Peggy Hall, Emma Hastings, Heather Junkins, Aoife McMahon, Annalisa Milano, Joannella Morales, et al. The new nhgri-ebi catalog of published genome-wide association studies (gwas catalog). *Nucleic acids research*, 45(D1):D896–D901, 2017.
- Carolina Medina-Gomez, Benjamin H Mullin, Alessandra Chesi, Vid Prijatelj, John P Kemp, Chen Shochat-Carvalho, Katerina Trajanoska, Carol Wang, Raimo Joro, Tavia E Evans, et al. Genome wide association metanalysis of skull bone mineral density identifies loci relevant for osteoporosis and craniosynostosis. *MedRxiv*, pages 2021–11, 2021.
- Adam C Naj, Christiane Reitz, Farid Rajabli, Gyungah R Jun, Penelope Benckek, Giuseppe Tosto, Jin Sha, Congcong Zhu, Nicholas A Kushch, Wan-Ping Lee, et al. Multi-ancestry genome-wide association analysis of late-onset alzheimer’s disease (load) in 60,941 individuals identifies a novel cross-ancestry association in lrcc4c. *Alzheimer’s & Dementia*, 18:e065822, 2022.
- Sebastian Nowozin, Botond Cseke, and Ryota Tomioka. f-GAN: Training generative neural samplers using variational divergence minimization. In *Advances in Neural Information Processing Systems*, pages 271–279, 2016.

- Adam Paszke, Sam Gross, Francisco Massa, Adam Lerer, James Bradbury, Gregory Chanan, Trevor Killeen, Zeming Lin, Natalia Gimelshein, Luca Antiga, Alban Desmaison, Andreas Kopf, Edward Yang, Zachary DeVito, Martin Raison, Alykhan Tejani, Sasank Chilamkurthy, Benoit Steiner, Lu Fang, Junjie Bai, and Soumith Chintala. PyTorch: An imperative style, high-performance deep learning library. In *Advances in Neural Information Processing Systems*, pages 8024–8035. 2019.
- Khush Patel, Ziqian Xie, Hao Yuan, Sheikh Muhammad Saiful Islam, Wanheng Zhang, Assaf Gottlieb, Han Chen, Luca Giancardo, Alexander Knaack, Evan Fletcher, et al. New phenotype discovery method by unsupervised deep representation learning empowers genetic association studies of brain imaging. *medRxiv*, pages 2022–12, 2022.
- Godfrey D Pearlson, Jingyu Liu, and Vince D Calhoun. An introductory review of parallel independent component analysis (p-ica) and a guide to applying p-ica to genetic data and imaging phenotypes to identify disease-associated biological pathways and systems in common complex disorders. *Frontiers in genetics*, 6: 276, 2015.
- Shaun Purcell, Benjamin Neale, Kathe Todd-Brown, Lori Thomas, Manuel AR Ferreira, David Bender, Julian Maller, Pamela Sklar, Paul IW De Bakker, Mark J Daly, et al. Plink: a tool set for whole-genome association and population-based linkage analyses. *The American journal of human genetics*, 81(3):559–575, 2007.
- Julius Rönkkö, Svetlana Molchanova, Anya Revah-Politi, Elaine M Pereira, Mari Auranen, Jussi Toppila, Jouni Kvist, Anastasia Ludwig, Julika Neumann, Geert Bultynck, et al. Dominant mutations in *itpr3* cause charcot-marie-tooth disease. *Annals of Clinical and Translational Neurology*, 7(10):1962–1972, 2020.
- K. T. Schütt, P.-J. Kindermans, H. E. Saucedo, S. Chmiela, A. Tkatchenko, and K.-R. Müller. Schnet: A continuous-filter convolutional neural network for modeling quantum interactions. In *Proceedings of the 31st International Conference on Neural Information Processing Systems*, pages 992–1002, 2017.
- Stephen M Smith, Gwenaëlle Douaud, Winfield Chen, Taylor Hanayik, Fidel Alfaro-Almagro, Kevin Sharp, and Lloyd T Elliott. An expanded set of genome-wide association studies of brain imaging phenotypes in uk biobank. *Nature neuroscience*, 24(5):737–745, 2021.
- Hannes Stärk, Dominique Beaini, Gabriele Corso, Prudencio Tossou, Christian Dallago, Stephan Günemann, and Pietro Liò. 3d infomax improves gnns for molecular property prediction. In *International Conference on Machine Learning*, pages 20479–20502. PMLR, 2022.
- Cathie Sudlow, John Gallacher, Naomi Allen, Valerie Beral, Paul Burton, John Danesh, Paul Downey, Paul Elliott, Jane Green, Martin Landray, et al. Uk biobank: an open access resource for identifying the causes of a wide range of complex diseases of middle and old age. *PLoS medicine*, 12(3):e1001779, 2015.
- Benjamin B Sun, Stephanie J Loomis, Fabrizio Pizzagalli, Natalia Shatokhina, Jodie N Painter, Christopher N Foley, Megan E Jensen, Donald G McLaren, Sai Spandana Chintapalli, et al. Genetic map of regional sulcal morphology in the human brain from uk biobank data. *Nature Communications*, 13(1):6071, 2022.
- Aiham Taleb, Matthias Kirchler, Remo Monti, and Christoph Lippert. ContIG: Self-supervised multimodal contrastive learning for medical imaging with genetics. In *Proceedings of the IEEE/CVF Conference on Computer Vision and Pattern Recognition*, pages 20908–20921, 2022.
- Yonglong Tian, Chen Sun, Ben Poole, Dilip Krishnan, Cordelia Schmid, and Phillip Isola. What makes for good views for contrastive learning? *arXiv preprint arXiv:2005.10243*, 2020.
- Arno van Hilten, Steven A Kushner, Manfred Kayser, M Arfan Ikram, Hieab HH Adams, Caroline CW Klaver, Wiro J Niessen, and Gennady V Roshchupkin. Gennet framework: interpretable deep learning for predicting phenotypes from genetic data. *Communications Biology*, 4(1):1–9, 2021.
- V.N. Vapnik. An overview of statistical learning theory. *IEEE Transactions on Neural Networks*, 10(5): 988–999, 1999.

- Petar Veličković, William Fedus, William L. Hamilton, Pietro Liò, Yoshua Bengio, and Devon Hjelm. Deep graph infomax. In *International Conference on Learning Representations*, 2019.
- Tongzhou Wang and Phillip Isola. Understanding contrastive representation learning through alignment and uniformity on the hypersphere. In *International Conference on Machine Learning*, pages 9929–9939. PMLR, 2020.
- Xiao-Lan Wang and Lianjian Li. Cell type-specific potential pathogenic genes and functional pathways in alzheimer’s disease. *BMC neurology*, 21(1):1–18, 2021.
- Zhengyang Wang, Yaochen Xie, and Shuiwang Ji. Global voxel transformer networks for augmented microscopy. *Nature Machine Intelligence*, 3:161–171, 2021. doi: 10.1038/s42256-020-00283-x.
- Junhao Wen, Ilya Nasrallah, Ahmed Abdulkadir, Theodore Satterthwaite, Guray Erus, Timothy Robert-Fitzgerald, Ashish Singh, Aristeidis Sotiras, Aleix Boquet-Pujadas, Zhijian Yang, et al. Mega-analysis of brain structural covariance, genetics, and clinical phenotypes. *Research Square*, 2022.
- Tete Xiao, Xiaolong Wang, Alexei A Efros, and Trevor Darrell. What should not be contrastive in contrastive learning. In *International Conference on Learning Representations*, 2020.
- Ziqian Xie, Tao Zhang, Sangbae Kim, Jiaxiong Lu, Wanheng Zhang, Cheng-Hui Lin, Man-Ru Wu, Alexander Davis, Roomasa Channa, Luca Giancarlo, et al. igwas: image-based genome-wide association of self-supervised deep phenotyping of human medical images. *medRxiv*, 2022.
- Kenji Yano, Yoichi Morinaka, Fanmiao Wang, Peng Huang, Sayaka Takehara, Takaaki Hirai, Aya Ito, Eriko Koketsu, Mayuko Kawamura, Kunihiro Kotake, et al. Gwas with principal component analysis identifies a gene comprehensively controlling rice architecture. *Proceedings of the National Academy of Sciences*, 116(42):21262–21267, 2019.
- Jure Zbontar, Li Jing, Ishan Misra, Yann LeCun, and Stéphane Deny. Barlow twins: Self-supervised learning via redundancy reduction. In *International Conference on Machine Learning*, pages 12310–12320. PMLR, 2021.
- Michael Zhang, Nimit Sharad Sohoni, Hongyang R Zhang, Chelsea Finn, and Christopher Ré. Correct-n-contrast: A contrastive approach for improving robustness to spurious correlations. In *NeurIPS 2021 Workshop on Distribution Shifts: Connecting Methods and Applications*, 2021.
- Bingxin Zhao, Tengfei Li, Yue Yang, Xifeng Wang, Tianyou Luo, Yue Shan, Ziliang Zhu, Di Xiong, Mads E Hauberg, Jaroslav Bendl, et al. Common genetic variation influencing human white matter microstructure. *Science*, 372(6548):eabf3736, 2021.
- Mohammadreza Zolfaghari, Yi Zhu, Peter Gehler, and Thomas Brox. Crossclr: Cross-modal contrastive learning for multi-modal video representations. In *Proceedings of the IEEE/CVF International Conference on Computer Vision (ICCV)*, pages 1450–1459, October 2021.

## A Data Processing and Split

All MRIs were linearly registered (affine registration with 12 DOF) to standard MNI152 space using the UKBiobank-provided transformation matrix with FSL FLIRT (Jenkinson et al., 2002) and all the outputs are of shape  $182 \times 218 \times 182$ . Large portion of the UKBiobank population are white British. In order to maximize the power of genetic discovery and avoid the complication of population stratification, the genetic association study was only done on the white British (UKBiobank data field 21000 and 22006) cohort. So we selected 6,130 images from subjects of mixed ethnicities (all non white British samples plus a small number of random white British samples) not overlapped with the samples for the genetic discovery to do the train and validation, among which 4,597 was randomly selected for training and 1,533 for validation. We used two quality metrics “inverted contrast-to-noise ratio” (UKBiobank data field 25735) and “Discrepancy between T2 FLAIR brain image and T1 brain image” (UKBiobank data field 25736) to ensure the quality of the training data.

Details about the evaluation metrics are provided below.

**Number of Loci** We perform genome-wide scans over 658,720 directly genotyped SNPs<sup>1</sup> and on 28,489 white British participants unseen during training. We use BOLT-LMM (Version 2.3.4) (Loh et al., 2015) for running GWAS. Age, gender, and the first 10 ancestral principal components are used as covariates. We use Bonferroni corrected p-value threshold of  $5e-9$  and a minor allele frequency threshold of 1% to get the significant SNPs and filter out the rare variants. We then cluster the significant SNPs into loci using a 250 kb window, which is approximately 0.25 cM (Elliott et al., 2018). The number of loci indicates the amount of genetic contribution to the learned features.

**Heritability** measures the proportion of variation of the feature explained by the genetic factors. It provides insight into the genetic basis of a feature. A higher heritability indicates that the representation is better associated with the genetic data. The heritability is computed using LDSC v1.0.1 (Bulik-Sullivan et al., 2015).

**Mutual Information** We estimate the mutual information between MRI representations and genetic data on the test set to explicitly demonstrate that the proposed objective adds to the generalizability of captured associations to unseen pairs. We train individual JSE-based mutual information estimators with the same architecture described in Appendix B for different methods. We train the MI estimator until the contrastive loss converges and take the opposite of the converged value as the MI estimation for each model.

## B Implementation Details

**MRI encoders** The MRI encoder is constructed as a 3D convolutional network consisting of three residual blocks (Wang et al., 2021) connected by two downsampling operators with stride convolutions. The numbers of channel maps are 32, 64, and 128, respectively for the three blocks. The final representations are 128-dimensional computed by a dense layer upon flattened feature maps. When computing the reconstruction loss, we include additional 128-dimensional vectors computed from a multi-head attentive readout from feature maps, and the reconstruction is performed on the 256-dimensional representation after concatenation. However, dimensions from attention are not used in GWAS computation. This is to further prevent the encoder from learning too detailed patterns, possibly noise, that are non-generalizable to the test set.

**Genetic encoders** Our genetic encoder consists of three 1D swin-transformer blocks connected by two down-sampling operators with a down-sampling rate of 10. The positional encoding for SNP physical positions is 128. The embedding dimensions are 32, 64, and 128 for the three blocks, respectively. The window size to perform attention is 10 and the number of heads is 4 for all self-attention operators. The downsampling operator computes the attention with learnable queries within each window, where the window size is equal to the downsampling size. The global pooling operators compute attention with learnable queries among all positions at multiple scales and resolutions.

<sup>1</sup>Applied Biosystems UK BiLEVE Axiom Array, UKBiobank data field 22438

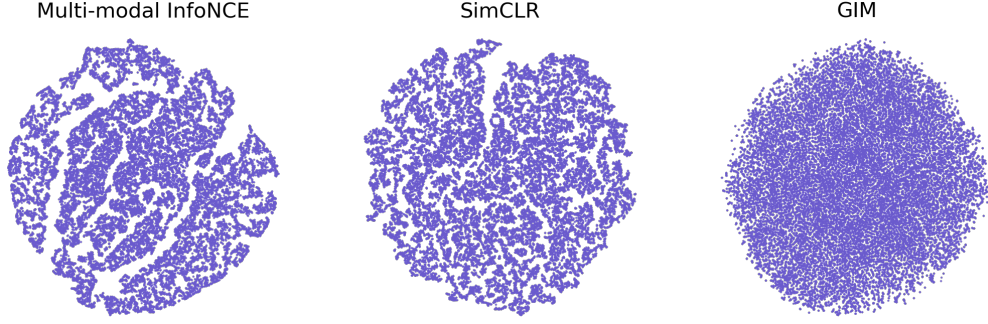


Figure 5: Visualization of learned representations with t-SNE. Forming clusters is not desired in the GWAS setting. Instead, a higher uniformity better utilize the space capacity and could lead to better GWAS discovery.

**Training** The models are implemented with PyTorch (Paszke et al., 2019) and are trained on a single Nvidia A100 GPU. The training is performed with the Adam optimizer (Kingma and Ba, 2014), cosine annealing scheduler (Loshchilov and Hutter, 2016) with a starting learning rate of 0.001 and the mini-batch size of 12. We simply set  $\lambda$  in the objective to 1 and do not exhaustively tune it. During training, we randomly crop the 3D MRI into smaller patches of size  $[160, 160, 160]$ . We first train the models with the genetic encoder frozen for 200 epochs, then include the augmentation on genetic data and continue training for additional 100 epochs, and finally co-train both MRI and genetic encoders and projection heads for 50 epochs with augmentation on genetic data. To perform augmentation, the genetic data has a probability of 0.2 to be randomly cropped and a probability of 0.8 to be evenly down-sampled into a length of 65,000.

**Baseline approaches** For Gen Prediction, we apply a linear layer to the output representation as a prediction head  $h^g : \mathbb{R}^q \rightarrow |G|$  to predict the class of each genotype in the genetic data and optimize the following loss.

$$\mathcal{L}_{\text{GenPred}} = \text{Cross-Entropy}(h^g(f_\theta(\mathbf{Y})), \mathbf{d}).$$

For baseline trans-modal contrastive methods, we follow the architecture, training loss, and training settings in Taleb et al. (2022). For the MRI augmentations, we perform the random flipping and rotation on the x-z plane, along with the random 3D patching. However, we found the flipping and rotation do not help on the GWAS performance in the 3D MRI case. For correlated InfoNCE, we compute the covariance matrix of learned MRI representations and minimize its difference with the identity matrix,

$$\mathcal{L}_{\text{decor}} = \|\hat{\mathbf{z}}^T \hat{\mathbf{z}} - \mathbf{I}\|^2,$$

where  $\hat{\mathbf{z}}$  is the normalized MRI representations in the mini-batch. Since the mini-batch size is small due to memory constrain, the covariance estimation can be less accurate, still leading to reduced performance.

## C Distribution of learned representations

We visualize the distribution of representations learned by trans-modal InfoNCE, SimCLR, and GIM, respectively, with t-SNE in Figure 5. Compared to baseline approaches, GIM learns representations that are more uniformly distributed in the space. According to the discussion on the difference between learning goals, the goal of our representation learning is not to form clusters for downstream classification purposes but to uniformly encode as much information about the genetic data as possible (Wang and Isola, 2020). Under this setting, clusters of representations are not desired and may harm the GWAS performance due to reduced capacity for other characteristics.

## D Gene mapping and query for previous known associations

We mapped significant SNPs to genes using Plink v1.9 (Purcell et al., 2007), and we presented the genes that are associated with the most significant new SNP of each model in the ablation study in Table 2. *CENPW*

is known to be associated with neurogenesis (Aygün et al., 2021) and cortical morphology (Sun et al., 2022), *WNT16* with skull and brain shape (Gori et al., 2015; Medina-Gomez et al., 2021), *ITPR3* with neuropathy (Rönkkö et al., 2020) and many psychiatric disorders (Cabana-Domínguez et al., 2022) and *MSRB3* with Alzheimer’s (Adams et al., 2017). For each unique locus in the best-performing model, we did a range query using the GWAS Catalog (MacArthur et al., 2017) API for the previously identified brain-related associations and the result is shown in Figure 6. We also queried each locus in the result of the Big40 study (Smith et al., 2021; Elliott et al., 2018), which uses thousands of conventional image-derived phenotypes to do GWAS and we found a locus not presented in the Big40 study in Chromosome 2, base pair 218466221 to 218604356 (in hg19 coordinate). This locus is mapped to *DIRC3*, which has been shown to be associated with Alzheimer’s disease (Naj et al., 2022; Wang and Li, 2021). This showcases the potential of our method in capturing features missed by the traditional expert-defined pipelines.

For the heritability, we see that the score generally increases when adding each component to the model. The only exception is the co-training of MRI and genetic encoder. The decrease in  $h^2$  can be due to the inconsistency between the non-linear genetic encoder and linear model for  $h^2$  computation. In other words, the linear model used to compute  $h^2$  are unable to capture non-linear associations. This is also discussed in Appendix F.

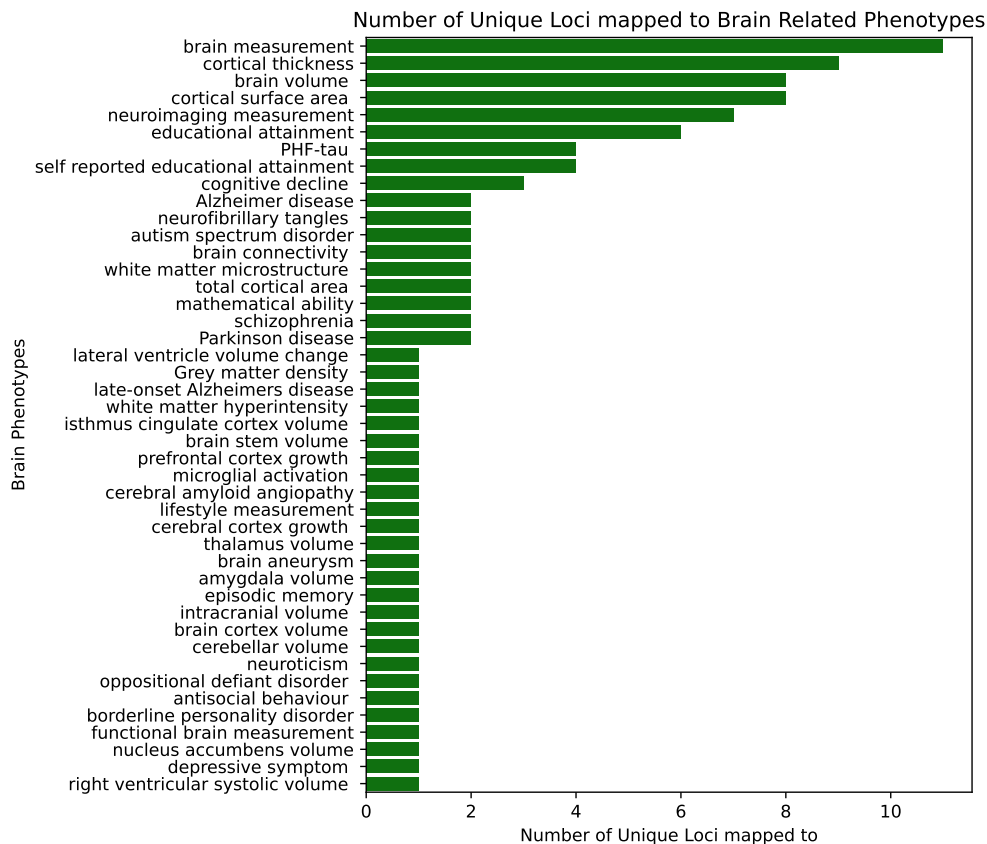


Figure 6: The number of unique loci found by the best model associated with a subset of brain-related traits in the GWAS Catalog.

## E Manhattan Plot of GIM results

The Manhattan Plot for loci discovered by GIM is shown in Figure 7.



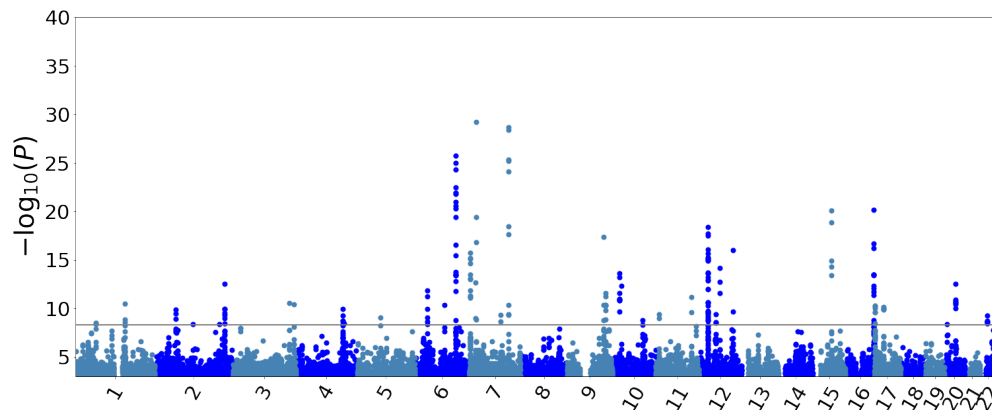


Figure 7: Aggregated Manhattan plot of the 10 PCs from the best model, the grey line represents the Bonferroni corrected p-value threshold of  $5e-9$ .

## F Limitations and Future Directions

Current GWAS relies on statistical testing based on linear models to identify significant loci and compute the heritability scores. However, these methods can be limited in their ability to capture non-linear and complex associations, leading to missed loci and inconsistencies between mutual information and other metrics. To address these limitations, new approaches to discovering and explaining non-linear associations are needed.

Regarding mutual information optimization, our current mutual information optimization solution aims to improve representations by capturing more generalizable associations, but it is still limited in reducing information on non-generalizable ones due to a lack of knowledge about non-generalizable patterns. With specific domain knowledge, it is possible to further improve these representations.